World Scientific
www.worldscientific.com

FP-LMTO simulation of the physical properties of arsenic-based binary XAs(X = Sc, and Al) compounds

Fatima Betraoui

*Computer Science and Mathematics Laboratory,
Physics Department, Faculty of Science and Applied Science,
Akli Mohand-Oulhadj University
Bouira 10000, Algeria*

Hamza Rekab-Djabri

*Laboratory of Micro and Nanophysics (LaMiN)
National Polytechnic School Oran, ENPO-MA, BP 1523
El M'Naouer 31000, Oran, Algeria*

*Faculty of Nature and Life Sciences and Earth Sciences
AMO University, Bouira 10000, Algeria*

Kamel Baddari

Ministry of Higher Education and Scientific Research, Algeria

Ahmed Azzouz-Rached [iD]*

*Magnetic Materials Laboratory, Faculty of Exact Sciences,
Djillali Liabes University of Sidi Bel-Abbes, Algeria
a.azzouzrached@univ-chlef.dz*

Mudasser Husain and Nasir Rahman

*Department of Physics, University of Lakki Marwat,
Lakki Marwat 28420, Khyber Pukhtunkhwa, Pakistan*

This paper presents a simulation of the structural and optoelectronic properties of Scandium Arsenide (ScAs) and Aluminum Arsenide (AlAs) compounds. Theoretical modeling was performed using *ab initio* first-principles calculations, specifically the density functional theory (DFT), and the Mindlab numerical software. The software used two methods: the full-potential muffin-tin orbital method (FP-LMTO) and the full-potential plane-wave method (FP-LAPW). These two methods are employed to solve the Schrödinger equation. The exchange correlation effects have been computed using two different approximations: the generalized gradient approximation (GGA) and the local density approximation (LDA). Our findings indicate that

---

*Corresponding author.

the zinc blende structure (B3) is the stable phase, while the Wurtzite phase (B4) is metastable for the AlAs compound. On the other hand, the ScAs compound crystallizes in the NaCl phase (B1). The AlAs compounds undergo three phase transitions: B3 → B4, B3 → B2 and B3 → B1. In contrast, ScAs does not undergo any transition. The obtained results for equilibrium energies, lattice parameters and gap energies are in closer agreement with the experimental and theoretical data. The AlAs compound exhibits a semiconducting character, while ScAs exhibits a semi-metallic character. Additionally, the refractive index of these two compounds is similar to that of silicon, which is crucial for their application in photovoltaic cells.

Keywords: DFT; FP-LMTO; GGA; LDA; phases transition; structural, electronic and optical properties.

PACS number: 31.10.+z

1. Introduction

The miniaturization of slides to nanometer dimensions requires a precise study of group III–V semiconductors. We have selected two binary compounds for numerical simulation to improve their physicochemical properties for various applications. Accurate results require an efficient calculation method, so we have used the FP-LMTO and FP-LAPW approaches, both of which use DFT. The exchange correlation effects were calculated using two different approximations: generalized gradient approximation (GGA) and local density approximation (LDA). Additionally, we used Mindlab, a sophisticated software package for this type of calculation. Aluminum Arsenide (AlAs) is a semiconductor material with an indirect gap X → Γ, making it well-suited for microelectronics. At room temperature, one of the main characteristics of the compound (AlAs) is its low specific weight, with a density of 2,7. It also has high chemical and corrosion resistance, good electrical and thermal conductivity (around 60% that of copper), and high mechanical and yield strength with a specific elongation of over 12%.[1] Aluminum arsenide (AlAs) has a wide range of properties that make it suitable for various technological applications, especially in microelectronics. The semiconductor material discussed is currently utilized in the production of advanced optoelectronic devices, including laser diodes, photovoltaic cells, sensors, transistors, and photodetectors.[2] Harkati Kerboua[3] states that AlAs can be obtained through "vapor phase epitaxy", a technique used to grow semiconductor layers on gallium arsenide GaAs substrates with the same crystalline structure and properties as the material being grown. Additionally, the binary compound Scandium Arsenide (ScAs) has recently gained more attention. Oyama *et al.*[4] stated that materials with the NaCl (B1) structure have been well-studied for their thermal, optical, and mechanical properties. Therefore, the ScAs binary compound has significant potential for technological applications. ScAs is useful for constructing conductive layers between materials with poor conduction properties but with light emission, light energy absorption, or other properties due to its metallic behavior with direct energy band Γ → Γ.[5] Additionally, new studies have been conducted on the determination of phononic properties, as cited by Ugur *et al.*[6]

Yim *et al.*[7] conducted a scientific review of this remarkable material and its preparation, obtained by vapor phase epitaxy. Single crystal layers of ScAs are obtained by epitaxy on silicon substrates at 300°K. The paper is organized as follows: Sec. 2 provides a brief description of the method used, Sec. 3 presents the results and their discussion in terms of structural and electronic properties, and Sec. 5 presents the conclusions.

2. Simulation Methods

To simulate the structural and electronic properties of our binary compounds, we used the Mindlab scientific software[8] implemented by the lmtART code. This program was the first to be installed on Windows and Linux. This software tool is implemented using two approaches, the first of which (FP-LMTO), introduced by Savrasov,[9] treats interstitial zones and Muffin-Tin spheres. This is made possible by expanding the plane wave potential in these interstitial zones. The concept of this method used in the calculations is ideal for extracting pseudopotentials suitable for materials.[10] Its main advantage is the great simplicity of working with algebraic systems. What's more, this method can be used to calculate many complicated and cautious properties that need to incorporate a very large number of functions in order to describe the problem properly. This is particularly true of plane waves because in the cases that can be solved, the effect is extremely simple. FP-LMTO is still widely used in molecular dynamics simulations. The second approach is FP-LAPW, developed by Wimmer and Hamann,[11,12] its potential is defined by

$$V(r) = \begin{cases} \displaystyle\sum_{G} V_I^{Ge^{iGr}}, \\ \displaystyle\sum_{L} V_{MT}^L(r) Y_L(\hat{r}), \end{cases} \tag{1}$$

where $V_I^{Ge^{iGr}}$ is the potential in the interstitial region, and $V_{MT}^L(r)$ is the potential in the muffin tin radius.

The basic idea of this method is to add variation freedoms to the base inside the Muffin-Tin, so that it is not necessary to set the total energies equal to the band energies. This is achieved by using not only the radial solution of the Schrödinger equation, but also its derivative with respect to energy. According to Andersen[13] the concept of augmentation in the two linear methods LMTO and LAPW essentially works by dividing space into Muffin-Tin orbitals centered on several nuclei and interstitial regions. And so the linear function (augmented plane wave) (LAPW) uses plane waves and LMTO uses spherical functions.

Method FP-LMTO is introduced as part of the functional theory of density DFT, using the approximation of the generalized gradient GGA and the approximation of the local density LDA. These two theoretical approaches provided the solution that allowed the first basic quantum methods to develop and calculate total energy, energy band structure and DOS state density as well as all possible physical

properties with very satisfactory accuracy, except that the LDA approach gives unsatisfactory values for the bandgap width, slightly underestimates the bond distances and overestimates the cohesion energies. This produces errors in basic properties such as equilibrium geometries, vibrational frequencies and charge densities. The errors are even greater in the excitations, particularly the bandgap in materials with giant structures. Apart from the fact that the GGA approach somewhat improves on the results from the LDA approach in properties such as geometry, frequencies and charge density, as well as results in the bandgap or small interactions. Calculation times are generally about twice as long as with LDA.

Thanks to DFT, we have been able to calculate the total energy that depends totally on the electron density of a system with **n** free **electrons**. In fact, this theory is a different method of solving the Schrödinger equation, in which the electron density distribution plays a central role in the wave function. It is currently one of the most usable methods, mainly in calculations with crystals, where it gives the best results.

3. Simulation Analysis

3.1. *Structural properties*

The structural parameters and the stability of the structure are determined according to the Murnaghan equation.[7,14] Table 1 shows that the GGA approximation overestimates the values of the following parameters: E is total energy, V the equilibrium volume of the elementary mesh, a is the equilibrium constant, and B' the derivative of the compressibility modulus. On the other hand, the LDA

Table 1. Structural parameter evaluations of the AlAs and ScAs extracted from our results.

	Phases	E (Ry)	V (Å)^3	a (Å)	c (Å)	c/a (Å)	B (GPa)	B'
				AlAs				
B1	LDA	−5000,0112	36,6779	5,2724			99,8861	3,4649
	GGA	−5007,8946	38,8425	5,3940			95,9142	3,4287
B2	LDA	−4999,9675	34,8590	3,2666			82,3803	3,2722
	GGA	−5007,8602	36,7300	3,3296			79,7323	3,0837
B3	LDA	−5000,0297	46,1193	5,6468			85,4695	3,1646
	GGA	−5007,9205	48,6866	5,7241			84,8811	3,0426
B4	LDA	−5000,0274	44,7312	4,0107	6,4219	1,6012	76,7902	3,3325
	GGA	−5007,9195	46,0027	4,0307	6,5391	1,6222	88,8530	3,2939
				ScAs				
B1	LDA	−6041,3627	40,9843	5,4729			101,7985	3,0746
	GGA	−6050,8828	44,5587	5,6277			85,9109	3,0868
B2	LDA	−6041,2719	39,4488	3,4042			84,8811	3,6401
	GGA	−6050,7927	42,4418	3,4883			69,7290	3,6292
B3	LDA	−6041,2693	55,9488	6,0339			62,5207	3,6028
	GGA	−6050,8102	60,0762	6,2359			54,7240	2,7556
B4	LDA	−6041,2745	54,5659	4,2966	6,8273	1,5890	54,8711	3,2523
	GGA	−6050,8117	58,75512	4,3876	7,0486	1,6065	53,8414	2,9871

approximation underestimates tem. Murnaghan's equation of state is

$$E(V) = \frac{B_0 V}{B_0'} \left(\frac{(V_0/V)^{B_0'}}{B_0' - 1} + 1 \right) + E_0 - \frac{V_0 B_0}{B_0' - 1},$$ (2)

where the modulus of compressibility is given by

$$B_0 = V \frac{d^2 E}{dV^2}.$$ (3)

3.1.1. *Comparison of results for the AlAs compound*

Among the references that have studied the AlAs compound in its stable B3 phase, for example, the accuracies of the minimum energy are 0,57%, GGA and 0,067%, LDA. Compared with Ref. 15, experimentally Greene *et al.*[16,17] found lattice constant values between 5,66 Å and 5,77 Å using the LDA and GGA approximations, respectively. On the other hand, the experimental compressive modulus values according to Bornshtein *et al.*[18] were 82,00 Gpa and 76,41 GPa same reference for the derivative $B' = 4,16$. Concerning the B4 phase our calculated $\boldsymbol{u}$ parameter value is 0,384, similar to Ref. 15 value which was 0,380 with an accuracy of 0,01%. Returning to the total energy values, the difference between those of the B3 phase and those of B4 is 0,03 eV LDA and 0,06 eV GGA. Based on these miniature values, we can say that the B4 phase is a metastable structure in the AlAs crystalline material. Figure 1 shows that there are three phase transitions from B3 to B4, B3 to B2 and B3 to B1.

3.1.2. *Comparison of results for the ScAs compound*

Figure 2 compares the equilibrium energies and volumes of the different crystalline phases, considered for the analysis of the binary compound ScAs, and obtained by the two approximations LDA and GGA. The most stable structural phase found by both approaches is the Rocksalt NaCl phase (B1), which determines the general character of the ScAs compound, since it corresponds to the ground state. We compare our results for the structural parameters of ScAS in the B1 phase with those in Ref. 19. With respect to the lattice constant, we find a difference of 0,001 Å, i.e. 0,0001%. Moreover, with those of Ref. 20, we find, for the volume $\boldsymbol{V}$ (eV) 0,005%, for the modulus B (GPa) 0,01% and for its derivative B' of 0,04%. Concerning structure B4, according to Tebboune *et al.*[20] for the internal parameters ($\boldsymbol{c}/\boldsymbol{a} = 1,377$ Å and $\boldsymbol{u} = 0,374$). We took those of Ref. 21 which is $\boldsymbol{u} = 0,380$, our results lead to $\boldsymbol{c}/\boldsymbol{a} = 1,5890$ Å which is in agreement with $\boldsymbol{c}/\boldsymbol{a} = 1,601$ Å calculated theoretically. Figure 2 shows that there is a single-phase transition from B1 to B2.

3.2. *Thermodynamic properties and phase transition*

3.2.1. *Why structural phase transition?*

The idea of the transformation of one structure into another more stable structure highlights the new thermodynamic properties of crystalline materials. To describe the phase transition, the enthalpy as a function of pressure was calculated for each
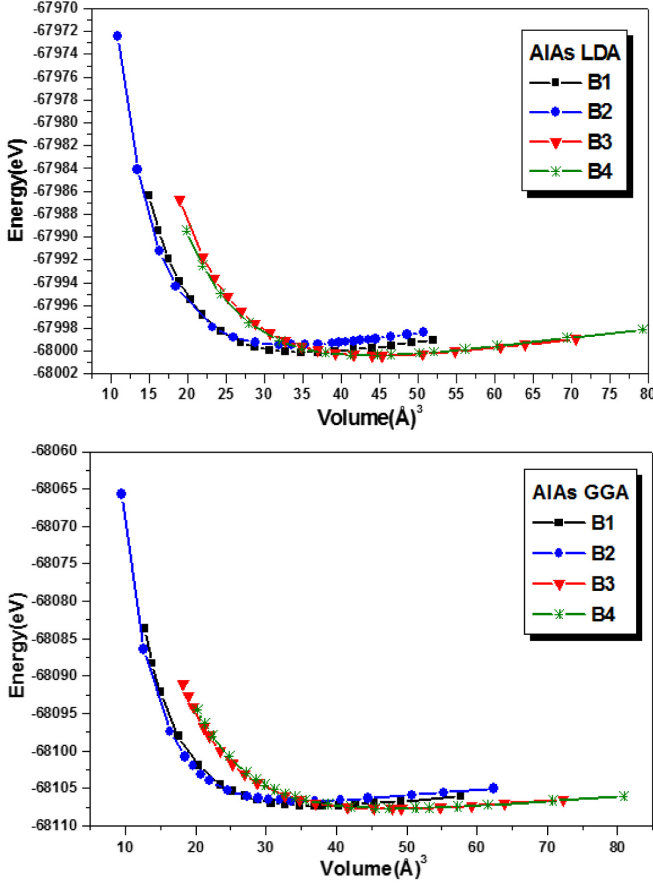
Fig. 1. (Color online) Total energy variation in relation to the AlAs material's unit cell volume in phases B1, B2, B3, and B4 as assessed by LDA and GGA.

structure at $T = 0°$K from the Gibbs free energy equation[22]:

$$G(P, T) = E + PV - TS \qquad (4)$$

with the term $(E + PV) = H$; where G is the Gibbs free energy as a function of pressure and temperature, H is the free enthalpy of the system as a function of equilibrium pressure and volume, and S is the entropy. To explain this concept, the equation linking the change in free energy to the changes in enthalpy and entropy of the process is given by

$$\Delta G = \Delta H - T\Delta S. \qquad (5)$$

The transition pressure was calculated by the following equation, according to Ref. 23:

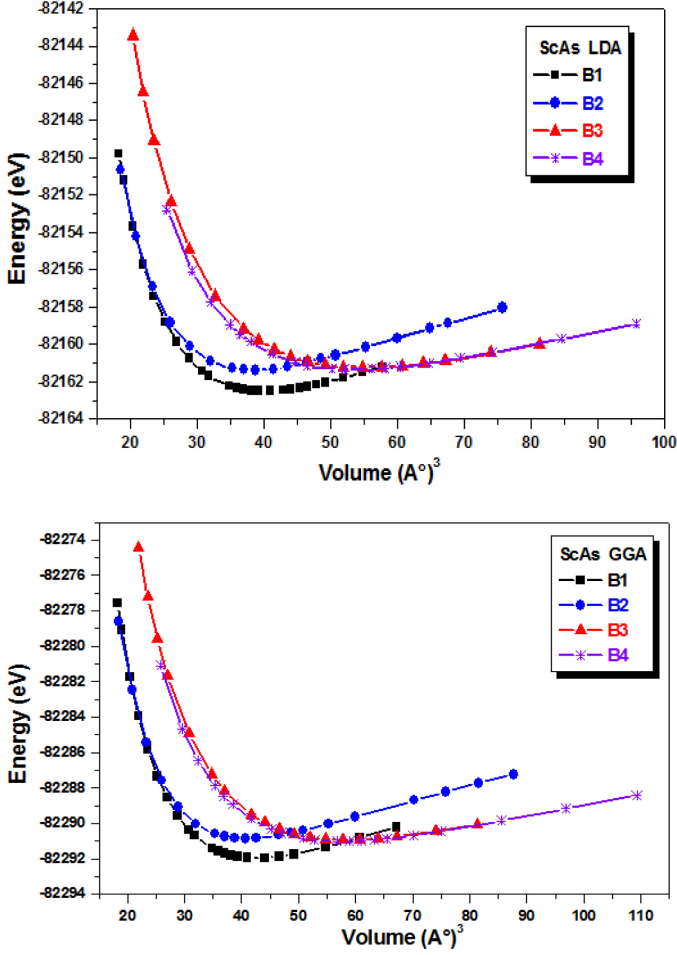$$P = \frac{B_0}{B'_0} \left[\left(\frac{V_0}{V} \right)^{B'_0} - 1 \right], \qquad (6)$$

Fig. 2. (Color online) Total energy variation in relation to the ScAs material's unit cell volume in phases B1, B2, B3, and B4 as assessed by LDA and GGA.

where B_0, B_0' and V_0 are successively the modulus of compressibility, its derivative and the equilibrium volume. These parameters were calculated at $T = 0°$ K and zero pressure.

3.2.2. *For the compound AlAs*

Figure 1 shows that the most stable structure is zincblende (B3), which has an equilibrium volume larger than the other three structures analyzed (Table 1) and that its minimum total energy value is closer to that of the NaCl (B1), CsCl (B2) and Wurtzite (B4) structures. The curve corresponding to the most stable phase (B3) crosses the three curves of the B1, B2 and B4 structures, explaining that three-phase transitions can occur between them.

Table 2.   Evaluation of phase transition pressures calculated by LDA and GGA of AlAs.

Transition	ΔV (Å)^3		Pression (GPa)		Autres valeurs LDA
	LDA	GGA	LDA	GGA	
B3 → B4	1,39	2,87	3,50	6,00	3,88 (Ref. 15)
B3 → B2	11,26	11,96	7,25	14,48	7,12 (Ref. 15)
B3 → B1	9,44	9,84	8,00	15,00	8,18 (Ref. 24)

Table 2 shows that our results are very similar to those of Refs. 15 and 24 concerning the transition pressure. Figure 3 shows the variation of enthalpy as a function of pressure, and there are three phase transitions between structures B3 → B4, B3 → B2 and B3 → B1. It illustrates that at a low pressure of 3,50 GPa, there is a phase transition between structure (B3) and that of Wurtzite (B4). In other words, above these pressure values, the enthalpy values are lower, indicating the relative stability of the said phase in this pressure range. It should be noted that the phase transition is highly dependent on the electronic structure of the material.
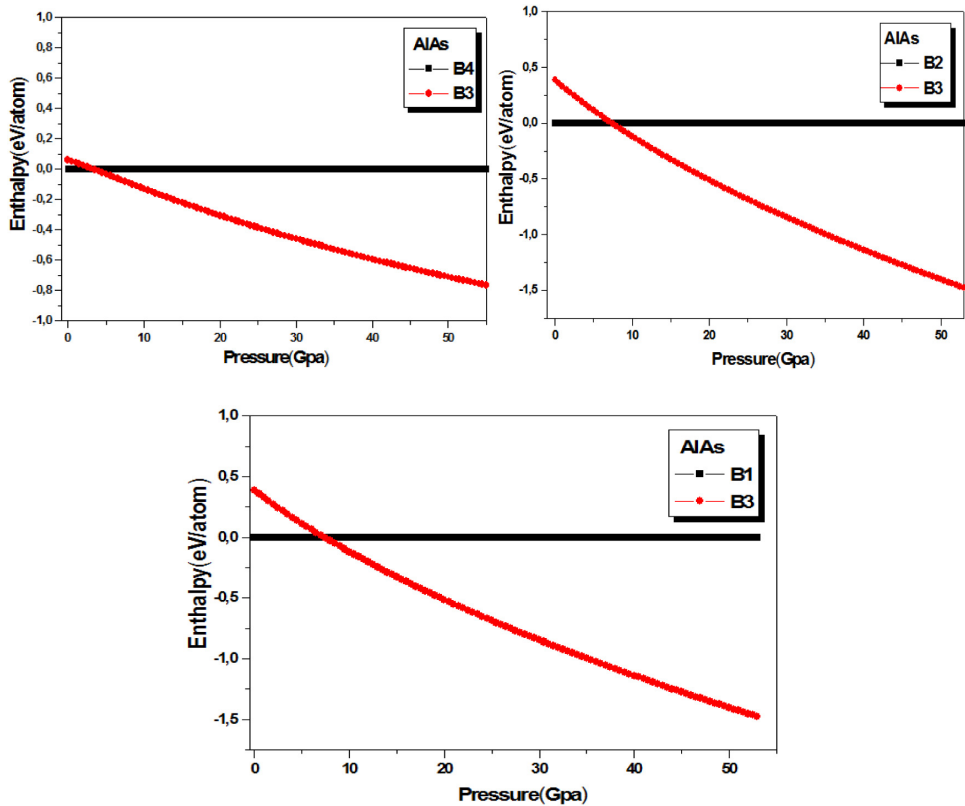

Fig. 3.   (Color online) Analysis of the enthalpy as a function of pressure, demonstrating the AlAs compounds' phase transition.

3.3. *Electronic properties*

3.3.1. *Band structures for the AlAs compound*

The band structure of the AlAs compound in its stable B3 phase is shown in Fig. 4, which shows that no valence band or conduction band energy level exceeds the fermi level E_F. The maximum of the valence band and the minimum of the conduction band are not at the same point of high symmetry, Therefore, the AlAs compound is a semiconductor material in which all the occupied energy bands are completely filled at absolute zero. And the last occupied band (valence band) is separated from the upper band (conduction band) by an energy bandgap $X \rightarrow \Gamma$ of the order of 1,78 eV and 1,51 eV by LDA and GGA, respectively, compared to 1,33 eV and 1,53 eV according to Ref. 15. In addition, compared with the other phases B1, B2 and B4, the AlAs compound exhibits metallic behavior because the conduction and valence bands exceed the Fermi level.

3.3.2. *Band structures for the ScAs compound*

The band structure plot of ScAs in the B1 phase is shown in Fig. 5, which indicates that ScAs is metallic in nature. It is in good agreement with the result previously predicted using FP-LMTO.[25] The bandgap is 1,25 eV in the direct energy band ($\Gamma \rightarrow \Gamma$). This is in good agreement with the previously reported theoretical work $E_g = 1,41$ eV. The small difference in bandgap is due to the choice of calculation method. The band structure of the ScAs compound shows that the material exhibits semi-metallic behavior. The two conduction and valence bands have energy levels
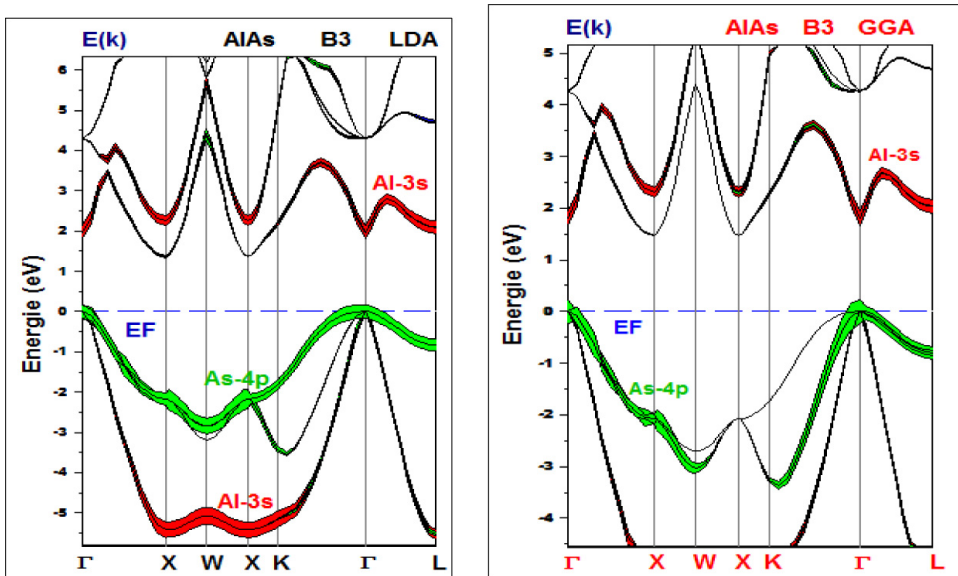

Fig. 4.   (Color online) Graphical presentation of the AlAs band structure in the B3 phase.
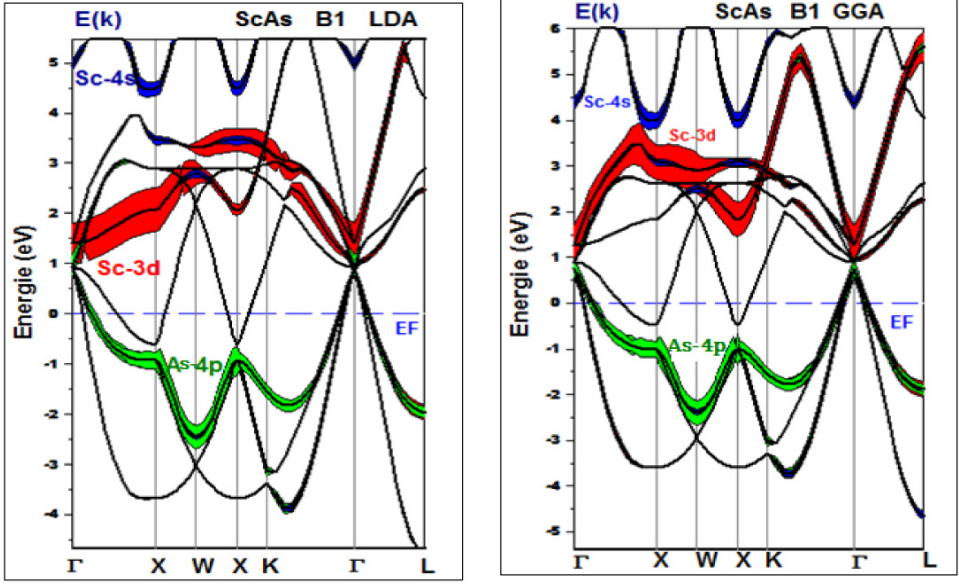
Fig. 5.   (Color online) The band structure of ScAs in B1 and AlAs in B3 phases, calculated by LDA and GGA.

above the Fermi level E_F, i.e. by an overlap of about 0,55 eV. Due to its metallic behavior, ScAs is useful for the construction of conductive layers. On the horizontal axis, the k vectors are recorded along certain directions of high symmetry in the first Brillouin zone. The Fermi level has been taken as the zero energy.

3.3.3. *Density of states for the AlAs compound*

Figure 6 shows that there are no electronic states at the Fermi level (0 eV). The same figures also reveal that, in both the valence and conduction bands, the orbital that contributes most to the total DOS is **3s-Al**, with its largest peak indicating the presence of states located in a narrow energy region, where the 3s-Al state is predominant and the **4p-As** state is present in a minority certainly due to the fact that the **As** atom is heavier than the **Al** atom. The same states occur in the conduction band where the energy peaks indicate well-located states.

3.3.4. *Density of states for the ScAs compound*

Concerning the density of states (Fig. 7), it can be added that **Sc-d** is the one that contributes most to the total DOS, presenting its largest peak at about 3 eV, which explains the excellent location of the states in a narrow energy window. The d-state is mainly found in the conduction band, with the energy peaks indicating states that are well located within an energy window in the DOS plot. The contribution of the orbitals of the **Sc** and **As** materials, where Fig. 7 shows that the **4p-As** orbital dominates in the valence band. Conversely, the **Sc-3d** orbital contributes
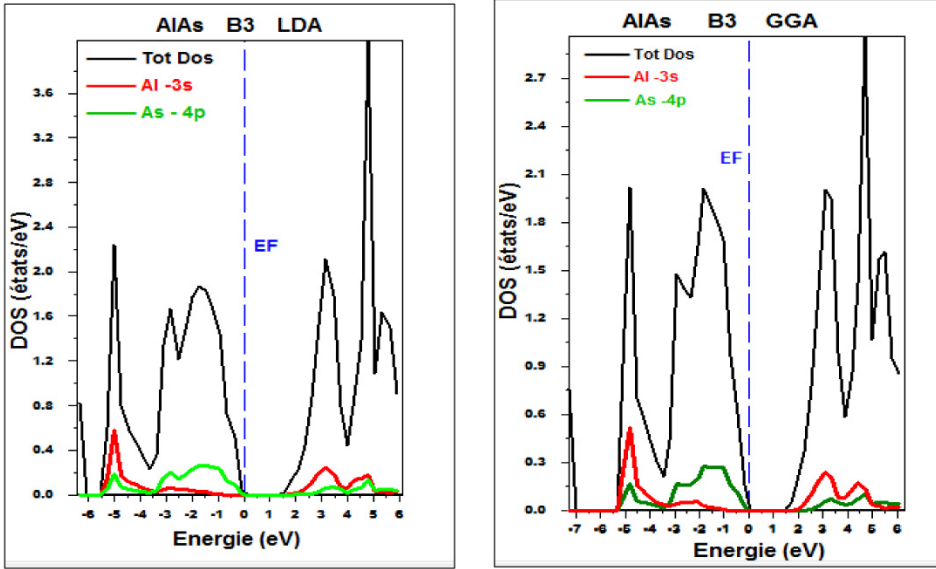
Fig. 6.   (Color online) Total density of states (TDOS) and partial density of states (PDOS) of AlAs in B3.

enormously in the conduction band and to a lesser extent in the valence band. Hence the existence of a hybridization between the **4p-As** and **3d-Sc** orbitals. It has been shown that the lattice constant has an enormous influence on the electronic and optical properties.
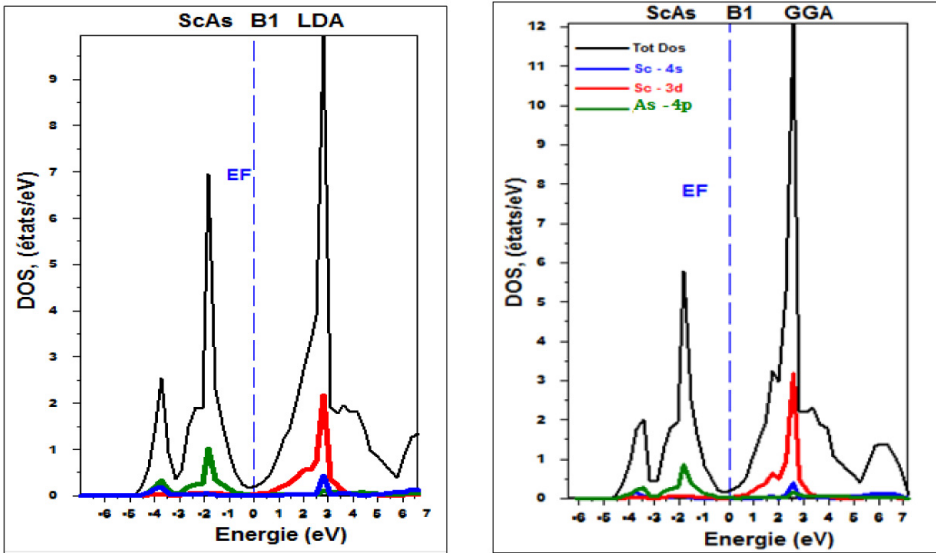

Fig. 7.   (Color online) Total density of states (TDOS) and partial density of states (PDOS) of ScAs B1phase.

3.4. *Thermal properties (melting point)*

As we already know, elastic properties are strongly dependent on thermal properties, in particular the melting point (***Tm***) and Debye temperature (***θ_D***) of semi-conductors.[26–28] This melting point is calculated by the following equation[27]:

$$Tm = 9.3\,\text{B} + 607, \tag{7}$$

where ***B*** is the modulus of compressibility. Our results gave for the binary compound **AlAs** in structure ZB (B3): 1401,778 and 1396,384 K, respectively by LDA and GGA. While for the binary compound **ScAs** in the Rocksalt structure (B1): 1553,647 and 1405,963, respectively by LDA and GGA. Unfortunately we were unable to make a comparison because this melting point was not reported in the literature.

3.5. *Characteristics of optics*

The optical properties are characterized by the dielectric function, the absorption coefficient, the function of electron energy loss and refractive index. In addition, the optical properties, like all properties are influenced by pressure and temperature.

The dielectric function $\varepsilon(\omega)$ describes the behavior of the material when excited by a light beam and comprises two parts, the imaginary part $\varepsilon_{\text{Im}}(\omega)$ and the real part $\varepsilon_{\text{Re}}(\omega)$ which is the derivative of the imaginary part. The formula for the total dielectric function according to Refs. 29 and 30 is given by

$$\varepsilon(\omega) = \varepsilon_{\text{Re}}(\omega) + i\varepsilon_{\text{Im}}(\omega), \tag{8}$$

where the real part is written as

$$\varepsilon_{\text{Re}}(\omega) = \frac{1}{\pi}\wp \int_{-\infty}^{\infty} \frac{\varepsilon_{\text{Im}}(\omega')}{\omega' - \omega}\, d\omega', \tag{9}$$

$$\varepsilon_{\text{Im}}(\omega) = -\frac{1}{\pi}\wp \int_{-\infty}^{\infty} \frac{\varepsilon_{\text{Re}}(\omega')}{\omega' - \omega}\, d\omega', \tag{10}$$

where $\wp$ is the principal value

The electron energy loss function $L(\omega)$, interprets electron-material interaction and inelastic electron scattering in a material as a function of light excitation or temperature. These parameters are essential for understanding spectroscopy (study of the interaction between the material and electromagnetic radiation) and photoelectric (electrons ejected from the cross-section of the material when excited by light). However, the optical constants of most compounds are unknown in the energy range from 10 to 50 eV, where electron–solid interactions are strong.[31] This function is defined by

$$L(\omega) = \text{Im}\left[\frac{-1}{\varepsilon(\omega)}\right]. \tag{11}$$

For the AlAs compound: The real part (Fig. 7) of the optical spectrum of AlAs at zero pressure as a function of photon energy is strongly wavelength-dependent. Its maximum is reached at a photon energy of about 3,32 eV compared to 3,36 eV in

Ref. 32, and it also reaches a minimum below zero at a photon energy of about 4,92 eV. However, the imaginary part has a maximum at 4,13 eV and a minimum at 4.48 eV. On the other hand, the spectrum of the energy loss function $L(\omega)$. We observe the large peak at 10,10 eV compared to 9,50 eV of the same reference. Our results are similar to those measured and obtained experimentally by Shinotsuka *et al.*[33] It is for this reason that this material, which is so rich, has given rise to so many original studies.

For the ScAs compound: The real part (Fig. 8) of the optical spectrum of ScAs at zero pressure as a function of photon energy is strongly wavelength-dependent. Its maximum is reached at a photon energy of about 1,6 eV, and it also reaches a minimum below zero at a photon energy of about 4,44 eV. In the imaginary part, however, it has a maximum of 4,12 eV and a minimum of 3,52 eV. On the other hand, the spectrum of the energy loss function $L(\omega)$. We observe the existence of a larger peak in this spectrum, located around an energy of 8,48 eV, beyond which the energy loss decreases as the photon energy increases.
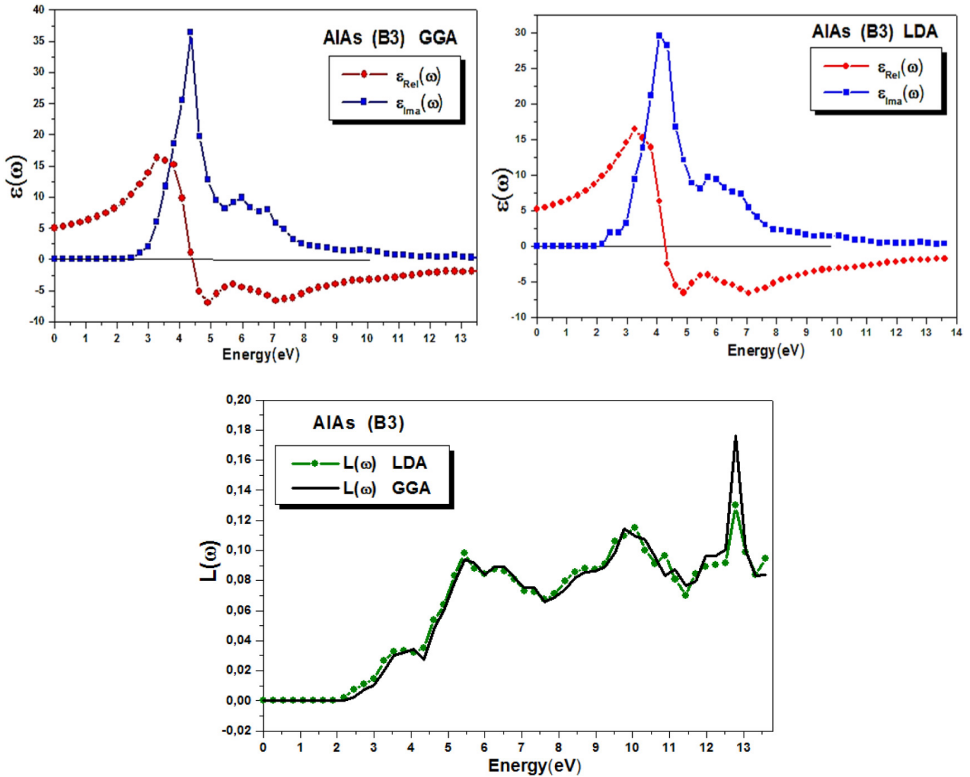

Fig. 8. (Color online) Graphical presentation of the dielectric functions imaginary $\varepsilon_{\text{Im}}(\omega)$, real $\varepsilon_{\text{Re}}(\omega)$ and the $L(\omega)$ electronic energy loss function of AlAs material at zero pressure.

The refractive index n of a material is one of the most important optical parameters.

Its study is a prerequisite in very distinct applications in optoelectronic structures such as optical fibers and solar cells. In this section, we will discuss different methods for calculating the refractive indices of AlAs and ScAs semiconductor materials.

The refractive index of the AlAs and ScAs compound is calculated by[34]

$$n(\omega) = \sqrt{\frac{\varepsilon_{\mathrm{Rel}}(\omega) + \sqrt{(\varepsilon_{\mathrm{Rel}}^2(\omega) + \varepsilon_{\mathrm{Im}}^2(\omega))}}{2}}. \tag{12}$$

In the case where $(\omega = 0)$, these are low frequencies, Eq. (12) will be

$$n(0) = \sqrt{\varepsilon_{\mathrm{Rel}}(0)}. \tag{13}$$

Our refractive index values are in agreement with those of the references cited above, and are summarized in Table 3.

According to our calculations of the optical properties, we have found that there is an optical transition from a transparent semiconductor to an absorbing semiconductor, in a photon energy range of 2.72 to 3.81 eV, For the two binaries AlAs and ScAs in their crystallization structures, i.e. in the Zincblende (B3) phase for aluminum arsenic and the Rocksalt (B1) phase for scandium arsenic. On the other hand, the refractive index is a principal parameter which depends on the imaginary part which explains the absorbance of light by the semiconductor and the real part which explains the transparency of the material. In addition, for the semiconductor to be a light-absorbing material, the value of the imaginary part must be greater than that of the real part, and this value will therefore be the optical transition point or simply the critical point, which has never been reported before in the literature for comparison purposes. This point will direct the two binary materials towards photovoltaic applications. Table 4 shows the optic transition points of the two binaries. In addition, it can be seen that the energy loss values are very small during excitation. Unfortunately we were unable to make a comparison because this transition point was not reported in the literature.

Table 3.   Variation in refractive index values for AlAs and ScAs B3 and B1.

Materials	E_g (eV)		n		Other result of n
	LDA	GGA	LDA	GGA	
AlAs	1.98	2.22	2.27	2.24	2.81 (Ref. 35)
					2.86 (Ref. 36)
ScAs	0.50	0.48	2.37	2.25	

Table 4.   Evaluation of the critical points of the optic transition of the ScAs and AlAs.

Materials	E(eV) photon		$\varepsilon_{\text{Img}}(\omega)$		$\varepsilon_{\text{Rel}}(\omega)$		$L(\omega)$	
	LDA	GGA	LDA	GGA	LDA	GGA	LDA	GGA
ScAs	2.99	2.99	8.44	8.71	7.65	7.72	0.067	0.064
AlAs	3.81	3.81	21.13	18.59	13.89	15.18	0.033	0.032
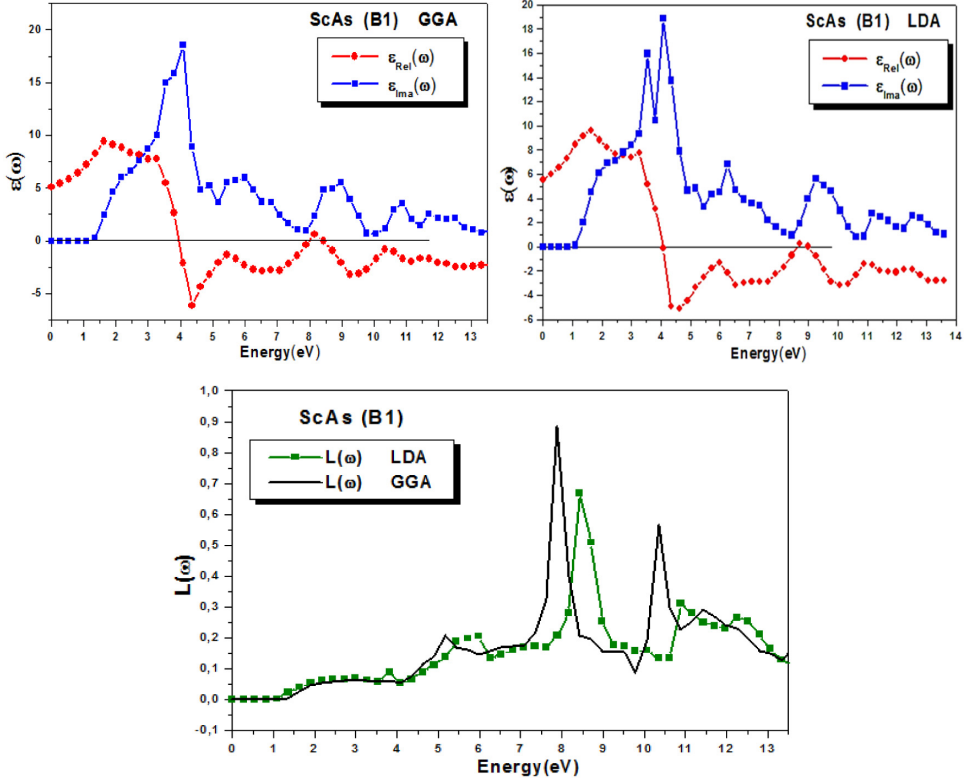
Fig. 9.   (Color online) The imaginary dielectric function, $\varepsilon\,\text{Im}(\omega)$, real dielectric function, $\varepsilon\,\text{Re}(\omega)$, and the electronic energy loss function, $L(\omega)$, of the ScAs material under no pressure are presented graphically.

4. Conclusion

The structural and electrical characteristics of AlAs and ScAs compounds in four distinct phases are covered in this paper: B1, B2, B3, and B4. The analysis predicts that the most stable crystalline structures for ScAs and AlAs compounds are B1 and B3, respectively. The AlAs compound may transition from B3 to B4, B2, and B1 phases, but there is no possibility of transition in the ScAs compound because the

B1 structure does not cross any of the known structures. For AlAs and ScAs, similar positive outcomes were observed in the computed parameters and experimental/ theoretical data that had previously been established by other authors. This work provides an excellent comparison between the two compounds using the LDA and GGA approximations.

We were able to find or calculate the melting point that characterizes the thermal properties of the two binary compounds AlAs and ScAs.

We were also able to find the critical points of the optical transition of the two binaries AlAs and ScAs, i.e. the points at which the semiconductor materials transform from a transparent material to an absorbing material. In addition, beyond that, we can say that these two semiconductor materials (good light absorbers) can be used for photovoltaic cell applications.

One last important point: Based on the ideal physical properties of the two semiconductor materials, we can propose a future study on a ternary compound from the AlAs/ScAs system, which will certainly be an ideal semiconductor.

ORCID

Ahmed Azzouz-Rached 🔵 https://orcid.org/0000-0003-4852-1000

References

1. K. Guler, l'aluminium et ses alliages, fabrication, emploi, BCV (1949).
2. J. N. Ruhstorfer *et al.*, *Nano Lett.* **18**(8), 5179 (2018).
3. C. Harkati Kerboua, Mécanismes de déformation de nanoparticules d'Au par irradiation ionique, Thèse de doctorat, p. 95 (2009).
4. S. T. Oyama, *Introduction to Transition Metal Carbide and Nitride Chemistry* (Virginia, USA, 1996).
5. S. Nicolas and P. William, *Rev. Tumbaga* **6**, 173 (2011).
6. S. Ugur and F. Soyalp, *Solid State Comm.* **147**, 198 (2008).
7. W. M. Yim, E. J. Stofko and R. T. Smith, *J. Appl. Phys.* **43**, 254 (1972).
8. http://www.physics.ucdavis.edu-mindlab/.
9. S. Y. Savrasov, *Phys. Rev. B* **54** (1996).
10. O. Ruben, Weht, Application of density functional theory to calculus of electronic properties in superconductors of high critical temperature, Thèse de doctorat, UBA (1995).
11. E. Wimmer *et al.*, *Phys. Rev. B* **24** (1981).
12. D. R. Hamann, *Phys. Rev.* (1979).
13. O. K. Andersen, *Solid State Commun. Phys. Rév. B* **12** (1975).
14. F. D. Murnaghan, *Proc. Natl. Acad. Sci. USA* **30**, 5390 (1944).
15. A. Srivastava and N. Tyagi, *High Pressure Behavior of AlAs Nanocrystal* (India, 2012).
16. R. G. Greene *et al.*, *Phys. Rév. Lett.* **72**, 2045 (1994).
17. S. M. Sze, *Semiconductor Device* (Université du Michigan, New York, 1981).
18. L. Bornshtein, Données numériques et relations fonctionnelles, in *Physique des éléments du groupe IV et des composés III – V*, Vol. 22 (Springer Verlag, Berlin, 1987).
19. R. Berger, *Acta Chem. Scand A* **31** (1977).
20. A. Tebboune *et al.*, *Phys. Status Solid B* (2006).

21. N. Farrer and L. Bellaiche, Properties of hexagonal ScN versus Wurtzite GaN and InN, (2002)
22. O. Arbouch *et al.*, *Comput. Mater. Sci.* **47**, 432 (2009).
23. D. S. Sholl and J. A. Steckel, *Density Functional Theory-A Practical Introduction* (John Wiley & Sons Inc., New Jersey, 2022).
24. S. T. Oyama, *The Chemistry of Transition Metal Carbides and Nitrides* (Virginia, USA, 1996).
25. V. Nayak and U. P. Verma, Study of Structural and Electronic Properties of ScN and ScAs in Rocksalt and Zincblende Structure: A DFT Approach, School of Studies in Physics, Jiwaji University, Gwalior-474011 (2015).
26. N. Bioud *et al.*, *Optik* **155**, 17 (2017).
27. S. Daoud *et al.*, *J. Nano- Electron. Phys.* **14**, 504061 (2013).
28. T. Özer, *Canad. J. Phys.* **98**, 357 (2020).
29. A. Gueddim, S. Zerroug and N. Bouarissa, *Luminescence* **135**, 243 (2013).
30. O. Stenzel, *Kramers-Kronig Relations in Springer Series in Surface Sciences* (Springer International Publishing, 2016).
31. R. H. Ritchie and A. Howie, *Philos. Mag.: J. Theor. Exper. Appl. Phys.* **36**(2), 463 (1977).
32. S. Rameshkumar, G. Jaiganesh, V. Jayalakshmi, (2015).
33. H. Shinotsuka, H. Yoshikawa and S. Tanuma **19**, 70 (2021).
34. T. Peng and J. Piprek, *Electron. Lett.* **32**, 2285 (1996).
35. M. J. L. Sangster, U. Schroder and R. M. Atwood, *J. Phys. C* **11**, 1523 (1978).
36. L. Boudaoud, Contribution à l'étude des Nanostructures, Thèse de Doctorat, Université M'sila (2010).